Chapter 12
Process Machine Interactions in Micro Milling

E. Uhlmann, F. Mahr, Y. Shi, and U. von Wagner

Abstract. In this chapter, both analytical and experimental studies on the process stability of micro milling are presented. The investigations are carried out in order to improve a comprehensive model, which describes interactions of the dynamic cutting forces and the dynamic machine tool behavior including the end mill. Dominant chatter frequencies at different operating points are determined by analyzing the process forces, acoustic signals as well as optical measurement signals. Results are documented and discussed by means of stability lobe diagrams. The findings are confirmed by analyses of the milled surfaces. Finally, some suggestions for improving the parameter identification are given.

12.1 Introduction

Significant Process Machine Interactions (PMI) can be observed in micro milling, e. g. by comparing the surface roughness of the manufactured workpiece to the vibration-response signals measured on the machine tool housing [18]. Alternating loads caused by interrupted cutting conditions interact with the flexible end mill and the machine tool structure. Deviations of the Tool Center Point (TCP) are the consequences.
In this context, a precise modeling of the interacting elements such as the machine tool structure, the end mill as well as the cutting conditions is necessary for process simulation. Stability predictions containing this information help to improve the machining of complex micro-structures.

Based on the experimental modal analysis of the machine tool structure and the operational vibration analysis of the micro end mill a comprehensive spatial multiple degrees of freedom (MDOF) model is described in this chapter. It is composed of oscillator chains and a flexible tool, which is modeled as a rotating Euler-Bernoulli beam using finite elements (FE).

The equations of motion are derived with Hamilton's principle including gyroscopic effects as a result of the rotational motion of the end mill. Besides, a self-excited part due to the internal material damping of the tool is included. The dynamic cutting forces, which occur during the process, are coupled to the MDOF model. Therefore, a geometrical milling force model is developed, which contains significant characteristics of micro cutting such as ploughing effects below the critical chip thickness.

B. Denkena and F. Hollmann (Eds.): Process Machine Interactions, LNPE, pp. 265–284.
springerlink.com

Experiments are carried out in order to verify the process stability behavior. The simulated and experimentally-determined stability lobe diagrams are then compared and analyzed in detail.

12.2 Modeling and Stability Prediction

Due to PMIs in micro milling it is not sufficient to model the end mill as a lumped mass for chatter prediction. Experimental modal analysis and operational vibration analysis are carried out in order to obtain the characteristics of the machine tool structure and the end mill.

Figure 12.1 shows a series of modal analyses conducted on a WISSNER Gamma 303 HP 3-axis micro milling machine tool. In all experiments, an electro-dynamic shaker is used to generate noise signal as excitation, which is measured with a piezo-electric force transducer. The response signal is measured with a tri-axial accelerometer.

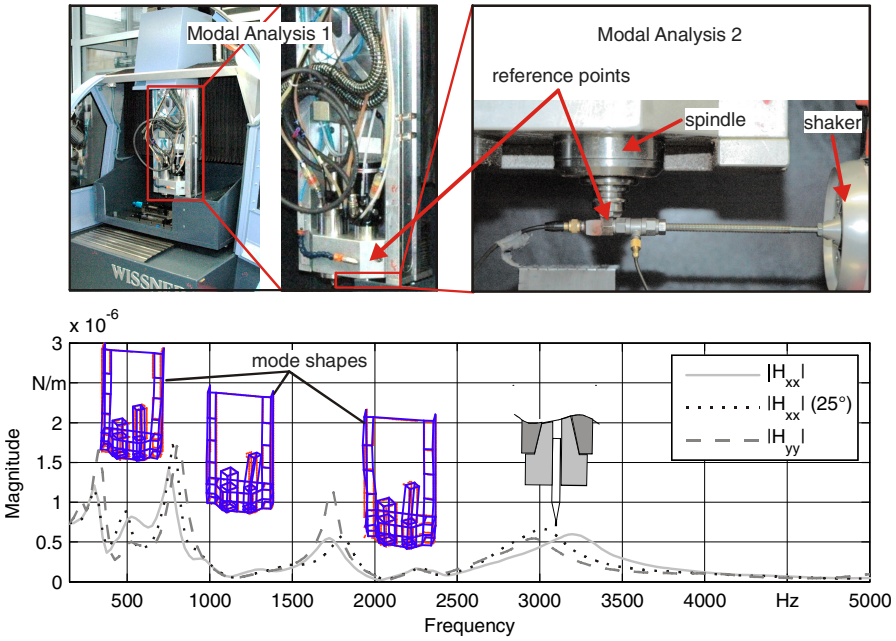

Fig. 12.1 Experimental modal analysis of the machine tool structure at different reference points

In modal analysis 1, the reference point is assigned to a location on the sliding carriage of the machine tool. The dominant mode shapes of the machine tool structure can be identified. However, the coherence at points on the tool shank is not sufficient. Therefore, the shaker and the accelerometer are mounted at the top of the tool shank to identify the frequency response functions (FRFs) at the tool

clamping. The measured FRFs in modal analysis 2 are shifted at different positions, where $|H_{xx}|$ (25°) means a 25-degree rotation of the Spindle-Tool Holder-Tool system (STT) from the initial measure position. All these phenomena indicate that the spindle configuration significantly affects the modal results of the system at non-rotating state. Considering the measured mode shapes, the first three natural frequencies of the FRFs can be traced back to the sliding carriage of the machine tool. The fourth mode is supposed to be caused by the clamping condition at the STT system. Considering the significant redundant mass effect of the accelerometer, the shaker and other unknown influences, the resonance frequency position and the damping factor of this mode are not reliable and not directly utilizable.

Due to the small dimensions of the micro end mill it is challenging to carry out a classical experimental modal analysis directly. Figure 12.2 shows an operational vibration analysis to study the resonance frequency of the tool.

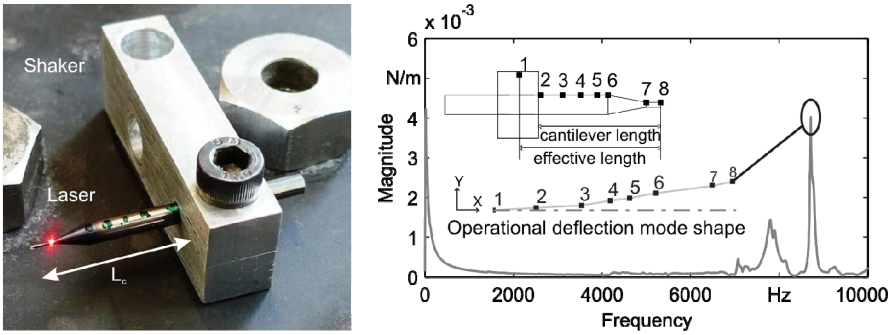

Fig. 12.2 Operational vibration analysis of the micro end mill with a shaker as excited base

An end mill with a nominal diameter of 0.5 mm and a cantilever length of 20 mm is clamped. The assembly is mounted on a large shaker, which produces noise signals as excitation. The excitation is measured with a tri-axial accelerometer. Several points, including one on the clamp, are measured with a laser vibrometer along the tool shank and the tip. The FRF (defined as response velocity/excitation acceleration) at tip point 8 is illustrated in Figure 12.2 (right). The first deflection mode shape corresponds to the dominant resonance at about 8.7 kHz. It should be noted that point 2 at the clamped end also exhibits a small transverse deflection, which means that the theoretical clamping point is located between points 1 and 2, and the effective cantilever length is more than 20 mm. This is caused by the imperfect clamping conditions of the simple assembly. However, it can be concluded that the first bending resonance frequency of the micro end mill with a cantilever length of 20 mm should be higher than 8.7 kHz [6, 8].

Compared to the models built with FRFs in the frequency domain the system models in the time domain are generally more complex. However, they also have advantages, e. g. there are more methods available for the modeling and an

analytical stability analysis. The complex dynamics of the system such as the rotation of the spindle-tool-system can be comprised. In this context, a spatial system model composed of oscillator chains and finite elements (FE) is utilized in order to incorporate both the machine tool modes and the flexible tool modes. Meanwhile, it also meets the requirements for process simulation and stability prediction.

In order to identify the system's parameters by an experimental modal analysis the model is firstly treated without rotational effects, i. e. regardless of the spindle speed and the according rotary inertia of the end mill. Subsequently, the rotational effects are taken into consideration within the formulation of the equations of motion for further application.

12.2.1 System Model without Rotational Effects

Without rotational effects, the equations of motion are decoupled in two orthogonal directions. Figure 12.3. shows the configuration of a simplified model, which describes the dynamic behavior at the tool clamping (see Fig.12.1. reference point 2). The tool is modeled by an Euler-Bernoulli beam with finite elements.

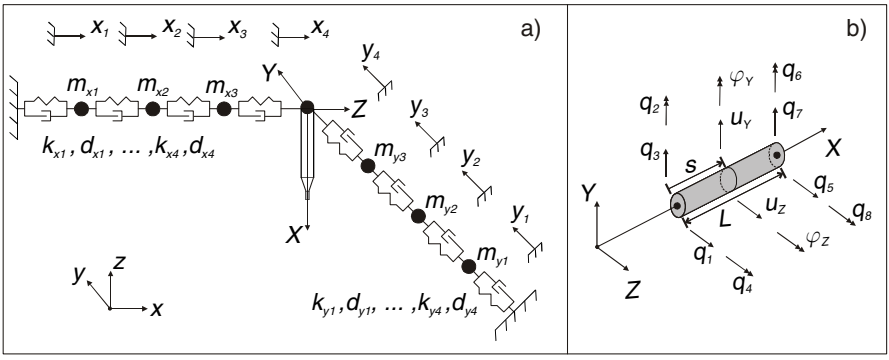

Fig. 12.3 a) Spatial system model; b) Finite element of the micro end mill

The global reference frame (xyz) is inertially fixed on the milling plane. Rotating this frame by 90° about the y-axis defines the non-rotating reference frame (XYZ) to simplify the description of the element kinematics while considering the rotational effects.

When using the time-dependent generalized coordinates

$$\mathbf{q_e}=(q_1, q_2, q_3, q_4, q_5, q_6, q_7, q_8)^T$$

at the two nodes of the element, the translational displacements of the element

$\mathbf{u_e}=(u_Z, u_Y)$
can be expressed as

$$\begin{pmatrix} u_Z \\ u_Y \end{pmatrix} = \begin{pmatrix} \phi_1 & -\phi_2 & 0 & 0 & \phi_3 & -\phi_4 & 0 & 0 \\ 0 & 0 & \phi_1 & \phi_2 & 0 & 0 & \phi_3 & \phi_4 \end{pmatrix} \mathbf{q}_e \,, \tag{12.1}$$

where the shape functions ϕ_1 to ϕ_4 can be found in [14].

For the Euler-Bernoulli beam the shear deformation is neglected. Thus, the rotations (φ_Y, φ_Z) and translations (u_Z, u_Y) are related by

$$\varphi_Y = -\frac{\partial u_Z}{\partial s}, \quad \varphi_Z = \frac{\partial u_Y}{\partial s} \,. \tag{12.2}$$

The system equations of motion can be derived using Hamilton's principle

$$\delta \int_{t_0}^{t_1} (T - U) dt + \int_{t_0}^{t_1} \delta W dt = 0 \,, \tag{12.3}$$

where T and U are the kinetic and potential energy of the system respectively, δW is the virtual work of non-conservative forces and δ represents the variational operator.

Because of the different geometries of the tool shank, the taper and the cutting edges at the tool tip, it is not accurate enough to model the micro end mills by a uniform beam. This can be demonstrated by the first three normalized bending mode shapes at different boundary conditions as shown in Figure 12.4. Note that the shank, tip lengths and diameters as well as the taper length considerably affect the natural frequencies and mode shapes of the tools [6]. In this case, a micro end mill with a cantilever length of 20 mm, a shank diameter of 3 mm, a nominal diameter of 0.5 mm and the tip length of 1 mm is used as a demonstration. It can be seen that the first bending mode is dominated by the shank. For clamped-free and sliding-free conditions they are similar to a uniform beam. The second and third bending modes are dominated by the taper, especially the tip deflections.

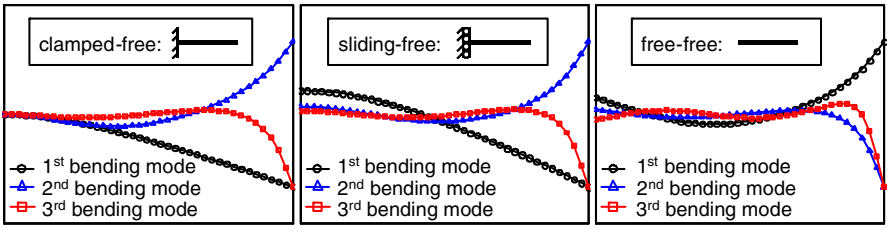

Fig. 12.4 Normalized mode shapes of the tool for different boundary conditions

To combine the modes of the tool and the machine, the parameters (mass, stiffness and damping) of the oscillator chains should be identified. Sub-structure coupling analysis is a useful method for this purpose. The detailed derivation of this method can be found in [12, 16]. Generally, the entire machine tool system is divided into two sub-structures: The complex machine tool structure including the upper part of the tool shank (FRFs can be measured by experimental modal

analysis) and the rest of the tool including the difficult to measure tool tip (FRFs usually obtained using beam theories or FE software). The identification of the FRFs at the coupling is challenging due to the rotational degrees of freedom (DOF). There are several methods to experimentally measure rotational FRFs or analytically derive them from measured translational FRFs [5]. To simplify the modeling the following assumptions are made.

For the analyzed micro milling machine tool, the clamping conditions between the end mill, the tool holder, and the spindle are perfect, i. e. sufficient clamping length and quasi-isotropic contacts. The rotational DOF can be neglected and the beam can be coupled to the oscillators with a sliding-free boundary condition. Since the measure point is approximately located at the contact position between the end mill and the tool holder, the effect of rotational DOF is supposed to be excluded. Moreover, a rigid coupling is adopted here, i. e. the rest of the end mill is coupled at the last oscillator without spring or damper elements (see Fig. 12.3).

In order to identify the parameters of the oscillators the system model is separately treated in the milling plane. In each direction, the parameters can be identified with the help of the measured and computed receptances using curve-fitting methods. A demonstration of two typical measurements in x and y-directions is shown in Figure 12.5. It should be mentioned that the identified oscillator parameters need to be furthermore optimized for chatter prediction, since the resonance frequencies and the damping factors are unverified especially at the fourth peak, which can be traced back to the clamping conditions at the tool shank.

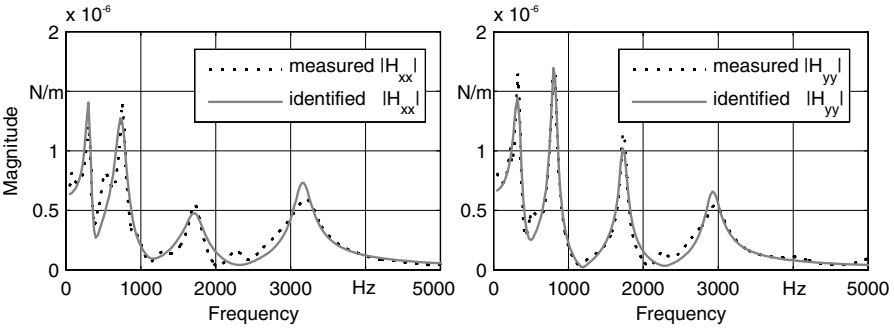

Fig. 12.5 Identified and measured FRFs

The mode shapes of the coupled system can be computed with the identified parameters of the machine tool modes. Figure 12.6 shows the fourth and fifth normalized mode shapes in y-direction.

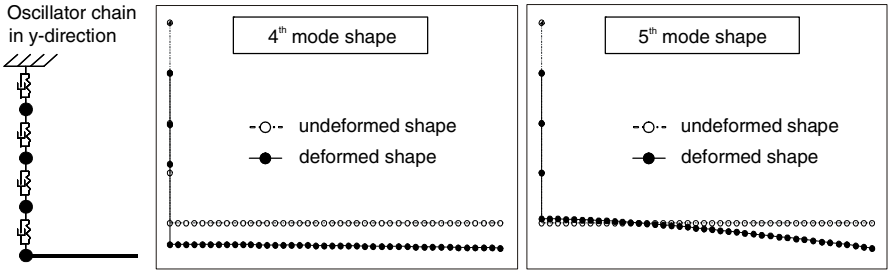

Fig. 12.6 Normalized mode shapes of the coupled system in y-direction

As seen, for this kind of system modeling the fourth mode is dominated by the oscillator chains including the tool as a rigid body. In contrast, the fifth mode includes a bending mode of the tool. Torsion, tension, compression effects and corresponding modes are not included here.

12.2.2 System Model with Rotational Effects

According to the oscillator chains configuration and the coordinate system selection, the rotational speed has no effect on the kinematics of the lumped mass. Thus, their equations are trivial and can be found in [17]. Here, attention has to be paid to the formulation of the finite element equations.

To describe the kinematics of the beam elements, a rotating frame ($x_1y_1z_1$) is attached on the neutral fiber of the beam. The rotation matrix (direction cosine matrix) between the fixed frame (XYZ) and the rotating frame ($x_1y_1z_1$) is defined by introducing two intermediate frames as well as three successive rotations:

1. φ_2 about Y defining the frame ($x_2y_2z_2$),
2. φ_3 about z_2 defining the frame ($x_3y_3z_3$),
3. φ_1 about x_3 defining the frame ($x_1y_1z_1$).

It is assumed that a non-holonomic constrain

$$\boldsymbol{\omega}_\mathbf{e} \cdot \mathbf{e}_X = \Omega \tag{12.4}$$

holds, where $\boldsymbol{\omega}_\mathbf{e}$ is the angular velocity vector of the beam elements with respect to the fixed frame, $\mathbf{e}_X$ is the unit vector of coordinate X in the fixed frame, Ω is the constant spindle's angular velocity. It should be pointed out that after linearization about small deformations, the rotations (φ_2, φ_3) can be substituted approximately by the rotations (φ_Y, φ_Z) shown in Figure12.3 b).

The total element's kinetic energy is composed of translational and rotational parts and can be expressed as

$$T_e = \frac{1}{2}\int_0^L \mu_e \mathbf{v}_\mathbf{e}^T \mathbf{v}_\mathbf{e} ds + \frac{1}{2}\int_0^L \boldsymbol{\omega}_\mathbf{e}^T \boldsymbol{\Theta}_\mathbf{e} \boldsymbol{\omega}_\mathbf{e} ds\,, \tag{12.5}$$

where μ_e is the mass per unit length of the finite element, the absolute velocity $\mathbf{v_e}$ is the derivative of $\mathbf{u_e}=(u_Z, u_Y)$ with respect to time in the non-rotating frame and $\mathbf{\Theta_e}$ is the mass moment of inertia of the element. While neglecting the shear and torsion deformations as well as the axial loads, the potential energy of the element can be expressed as

$$U_e = \frac{1}{2}\int_0^L EI_e \mathbf{u_e}''^T \mathbf{u_e}'' ds\,, \tag{12.6}$$

where E is the Young's modulus, I_e is the second moment of area of the element and

$$\mathbf{u_e}''=\partial^2 \mathbf{u_e}/\partial s^2. \tag{12.7}$$

The internal viscous damping of the tool is assumed to be proportional to the element bending stiffness EI_e with an introduced damping factor d_i [19, 21]. By variational calculation the linearized element's equations of motion are

$$\mathbf{M_e}\ddot{\mathbf{q}}_\mathbf{e} + \left(d_i\mathbf{K_e} - \Omega\mathbf{G_e}\right)\dot{\mathbf{q}}_\mathbf{e} + \left(\mathbf{K_e} + d_i\Omega\mathbf{K_{se}}\right)\mathbf{q_e} = \mathbf{f_e}\,, \tag{12.8}$$

where the element matrices are similar as stated in [14, 21]. It is noteworthy that a self-excited term arises due to the rotation and internal viscous damping of the tool, which differs from regenerative effects in cutting processes.

The assembled system's equations of motion consisting of the finite elements and oscillator's equations of motion are accomplished with the compatibility constraints at the corresponding element nodes. In total, the comprehensive model has 170 degrees of freedom (DOF). It should be noted that the system's equations expressed in the fixed frame have a simple matrix form due to the non-rotating oscillator chains. When they are transformed into the rotating frame, time-dependent terms ($\cos\Omega t$ and $\sin\Omega t$) appear in the oscillator-related components [17].

12.2.4 Process Model for Micro Milling

A complex geometrical model is implemented in order to calculate the dynamic cutting forces. Regarding the cutting process, one significant difference between macro and micro cutting is the influence of the cutting edge radius r_β. While in macro milling r_β is significantly smaller than the chip thickness h, in micro milling r_β is of the same order as h. Above the critical chip thickness h_{cr} shear deformation is dominant. Below this value elastic deformation becomes dominant and the effect of ploughing occurs [11].

Geometrical correlations can be used to estimate the critical chip thickness,

$$h_{cr} = r_\beta \cdot (1 - \cos\Theta_m) \tag{12.9}$$

where Θ_m is the critical angle, which can be determined from the negative effective rake angle γ_{eff} ($\gamma_{eff} = \pi/2 - \Theta_m$).

Empirical investigations from several researchers report a strong dependency of the workpiece material to the ratio h_{cr}/r_β as follows:

- micro cutting of copper values of 0.1 to 0.2 can be found in [13],
- aluminum and steel values of 0.25 and 0.38 are reported in [20].
- L'Vov [10] derived a neutral point of $\Theta_m = 45°$ independent from friction. In this case, with (12.8) h_{cr}/r_β is 0.293.

To predict the surface roughness the correlation

$$R_{kin} = \frac{d}{2} - \sqrt{\frac{d^2}{4} - \left(\frac{f_z}{2}\right)^2} \tag{12.10}$$

can be extended by the critical chip thickness as [3]

$$R_{th} = \frac{f_z^2}{4d} + \frac{h_{cr}}{2}\left(1 + \frac{d \cdot h_{cr}}{2 \cdot f_z^2}\right). \tag{12.11}$$

Figure 12.7 shows the critical chip thickness and the theoretical surface roughness based on the above-mentioned theories.

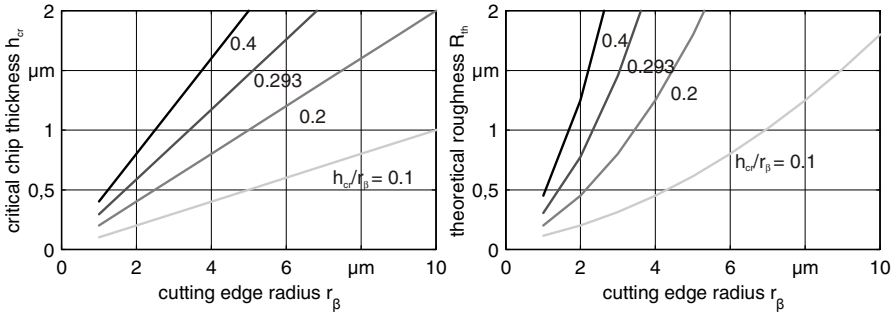

Fig. 12.7 Influence of the cutting edge radius r on the critical chip thickness h_{cr} (left) and on the theoretical surface roughness R_{th} (right)

Since the geometrical estimation of the surface roughness already indicates significant influence of the cutting edge radius, the cutting forces and the process stability are supposed to be affected as well [8]. Figure 12.8 shows a schematic view of the geometrical conditions at the cutting edge considering this point.

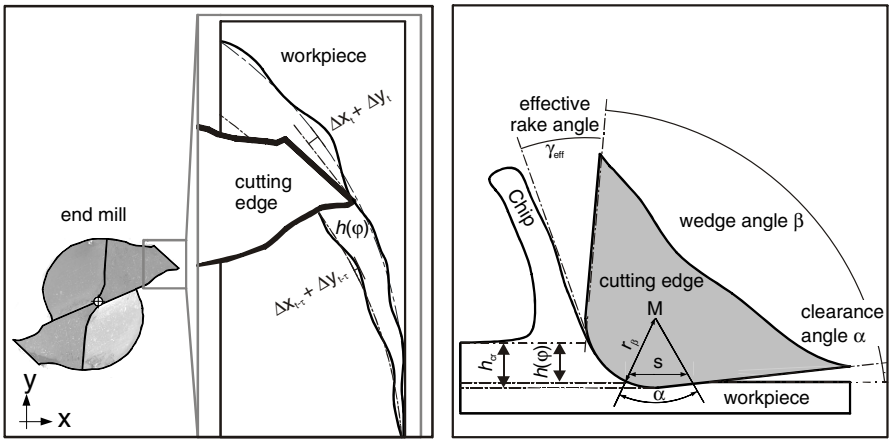

Fig. 12.8. Schematic view of the cutting force model

The chip thickness (12.12) can be described by a function of the rotation angle ϕ, which is divided into segments $\phi(z)$ in order to consider the helix angle λ of the end mill. Furthermore, information about the trochoidal cutting edge trajectory, self-induced and separately induced vibrations resulting in deflections are also included.

$$h(\phi) = \underbrace{f_z \cdot \sin(\phi)}_{h_{static}} + \underbrace{f_z \cdot n \cdot N_z \cdot \phi_{current}}_{h_{dynamic}} + \underbrace{\Delta x_{t-\tau} + \Delta y_{t-\tau}}_{h_{previous\ cut}} + \underbrace{\Delta x + \Delta y}_{\delta_{seperately\ induced}} \tag{12.12}$$

By multiplying (12.12) with a screen function $g(\phi)$ (1 or 0), as described in [4], the interrupted cutting conditions as they occur in milling can be set according to the cutting parameters. The volume below the critical chip thickness V_{pl} is also derived geometrically to take the ploughing effect into consideration.

$$V_{pl} = \left(r_\beta^2 \cdot \arcsin\left(2\sqrt{\frac{r_\beta^2 - \left(r_\beta - h_{cr}\right)^2}{2 \cdot r_\beta}} \right) - \sqrt{r_\beta^2 - \left(r_\beta - h_{cr}\right)^2} \cdot \left(r_\beta - h_{cr}\right) \right) \cdot \frac{d}{2} \tag{12.13}$$

The cutting forces in radial and tangential direction can now be calculated by

$$F_r = \sum_{z=0}^{z=a_p} \underbrace{\left(K_r \cdot a_p \cdot h_\phi^{\,x_f} \right)}_{cutting} + \underbrace{\left(K_{p,r} \cdot V_{pl} \right)}_{ploughing} \tag{12.14}$$

$$F_t = \sum_{z=0}^{z=a_p} \underbrace{\left(K_t \cdot a_p \cdot h_\phi^{\,x_f} \right)}_{cutting} + \underbrace{\left(K_{p,t} \cdot V_{pl} \right)}_{ploughing} \cdot \underbrace{\left(1 + \mu_f \right)}_{friction} \tag{12.15}$$

K_i and μ_f are specific constants which have to be determined through experiments or taken from appropriate literature. x_f describes the non-linear behavior of the specific force constants according to different ranges of the feed per tooth f_z [9].

In order to investigate the cutting edge effect experiments are carried out with different materials. The choice orients to commonly used materials in micro milling especially for the die and mold fabrication (e. g. powder metallurgic steel, AmpColoy). Figure 12.9 shows the specific force constants.

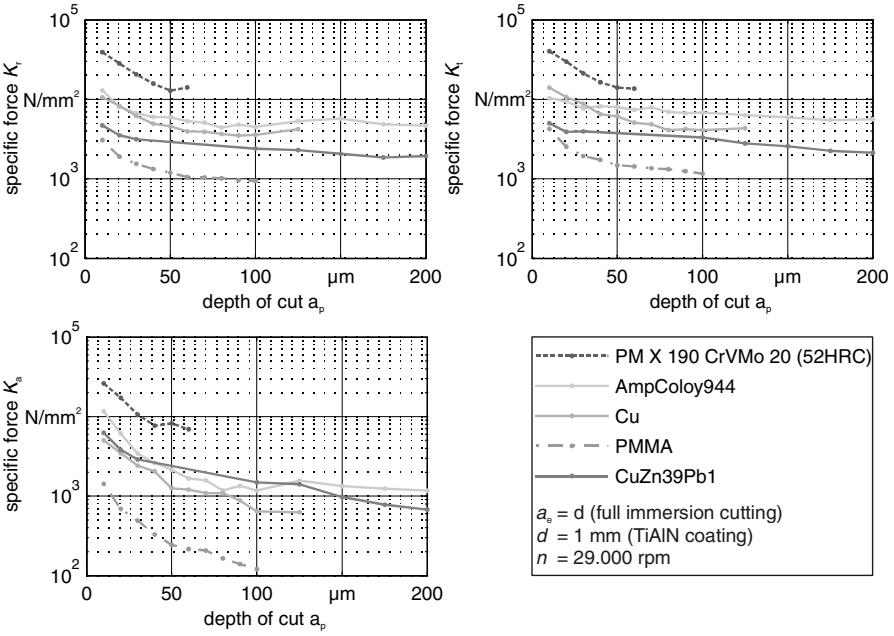

Fig. 12.9 Specific forces in radial, tangential and axial direction for different materials

To analyze the complex PMIs in micro milling, brass (CuZn39Pb1) is selected to be the most appropriate material. The specific force constants only possess minor non-linearities in a large field of operating points and lower tool wear can be estimated compared to hardened steel. Nevertheless, the cutting forces are high enough to evoke chatter.

At this point, the cutting forces can be calculated in radial and tangential direction. By applying the standard rotation matrix

$$\Theta_\phi = \begin{bmatrix} -\sin(\phi) & -\cos(\phi) \\ -\cos(\phi) & \sin(\phi) \end{bmatrix} \tag{12.16}$$

the cutting forces can be written in x and y- direction and compared to the measured process forces.

$$F_{xy} = \Theta_\phi \left[F_r \; F_t \right]^T \tag{12.17}$$

Figure 12.10 shows calculated cutting forces under variation of the helix angle (left) and the cutting edge radius (right).

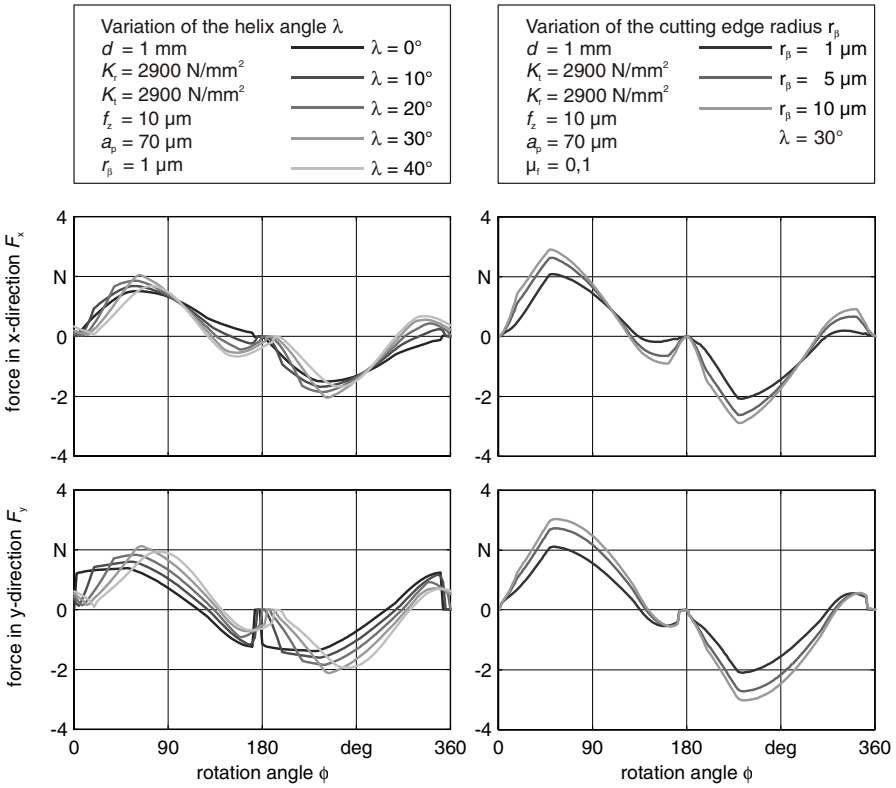

Fig. 12.10 Influence of the helix angle (left) and the cutting edge radius (right) on the cutting forces

The calculation shows a significant influence of these parameters. The sudden rise of the cutting forces at small helix angles is noticeable. Also, increased cutting forces due to a higher cutting edge radius can be seen, which is typical for wearing end mills. This means that neglecting these effects might cause strong divergences when simulating the cutting forces and applying them to the machine tool structure. Especially the dynamic excitation of the end mill is affected [15].

The above-described force model consists of the major influences, which occur in micro milling. However, because of its non-linear and complex character it is difficult to be transferred into the frequency domain. It is therefore rather predestinated for simulations in the time domain. Thus, for the following analyses in the time domain some simplifications are made:

- The feed per tooth f_z is constantly set to 10 µm, which reduces the influences of the ploughing effect,
- all experiments are carried out in full-immersion cutting to reduce high dynamic excitation frequencies at the entrance and exit of the cutting edge.

The used cutting force model corresponds to the implementations described in [4]. Solely the specific force constants K_i are adapted according to the varying depth of cut a_p and the adjusted spindle speed n (see Fig. 12.9).

12.2.5 Stability Prediction

Stability charts can be calculated to predict stable cutting processes and to improve the efficiency of the production. In macro-scale milling, two different types of instabilities can appear. They are referred to as (secondary) Hopf instability and period doubling (also flip instability). Period doubling usually occurs at low radial immersion and when using cutting tools with a small number of cutting edges. It is therefore under steady investigation for high speed cutting (HSC) processes. Several analytical methods for stability prediction have been successfully developed both in the frequency domain [1, 4] and in the discrete time domain [2, 7]. The methods vary regarding the required computing time, which strongly affects their efficiency when high-order DOF systems are analyzed. In this context, the FE model is only applied to the case of full immersion cutting. Thus, the zeroth-order-approximation method [1] is used.

For stability analyses, the linearized form of the cutting force at a stationary operation point, i. e. the constant feed rate, is coupled to the system equations of motion. The equations can be transformed into the frequency domain by approximating the force directional coefficients with only the zero order of their Fourier series. Although the spindle speed is explicitly involved in the governing delay-differential-equation (DDE) by the gyroscopic and internal damping terms, the change of the structural dynamics (i. e. FRF at tool tip point) due to the spindle speed can be neglected for the considered spindle speed range. Reasons for that are the non-rotating modeling of the oscillator chains and relatively small rotary inertia of the end mill.

12.3 Experimental Investigation

12.3.1 Experimental Set-Up

All experiments are carried out on a WISSNER Gamma 303 HP 3-axis milling machine tool using a Precise SC3062 high-frequency spindle with a maximum spindle speed of 60,000 rpm. Due to effects such as tool wear and premature tool breakage the micro milling process can still be seen as hardly reproducible. Therefore, only one type of end mill is used. The two-fluted end mills with a nominal diameter of $d = 1$ mm are TiAlN-coated and possess a helix angle of $\lambda = 30°$. All

experiments are conducted with brass (CuZn39Pb1) as workpiece material. To enable statistical analyses three tests are carried out at each operating point.

Different measuring devices are used to gather signals describing the process characteristics.

- the process forces are measured with a Kistler Dynamometer 9256C2,
- the acoustic characteristics are recorded with a conventional microphone (maximum sample rate: 16 kHz),
- the tool deflection and its velocity are measured with a Polytec Vibrometer OFV-353.

All signals are logged with a National Instruments data acquisition system NI9162–USB and signal-treated (e. g. FFT) with MATLAB.

12.3.2 Results

The verification of the calculated stability charts requires a reliable criterion for unstable process conditions. Therefore, it is common practice to divide measured signals into their spectral components by applying a Fourier transformation. In case of unstable process conditions chatter frequencies can then be detected. Figure 12.11 exemplarily shows the spectra of measured forces and microphone signals at a spindle speed of n = 28,000 rpm and increasing values of the depth of cut a_p from 60 µm to 105 µm.

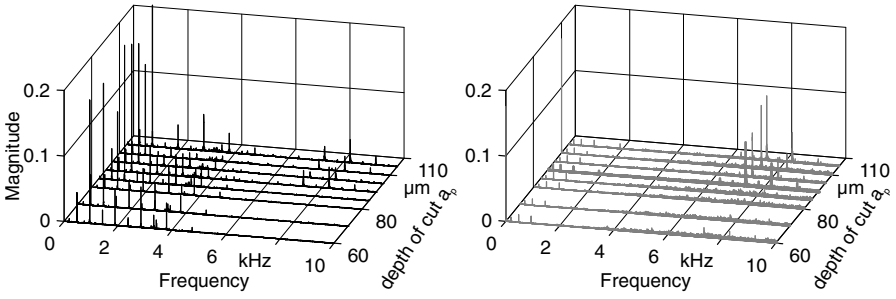

Fig. 12.11 Spectra of the force signals (left) and microphone signals (right)

Both signals clearly reveal typical chatter frequencies above an a_p-value of 90 µm. It is remarkable that almost all chatter cases come along with multi-chatter frequencies. However, high magnitudes above 6 kHz can only be found at unstable operating points. Their appearance is therefore used as a chatter criterion. Regarding the microphone signals it can be stated that the frequencies with greater magnitude are related to the dominant natural frequency of the STT system. Other frequencies arise from a combination between the basis chatter frequency and the tool engagement frequency. This phenomenon is usually observed in macro-scale milling with low radial immersion but not in full immersion cutting processes, where only the frequency around the most flexible mode is addressed for chatter

[1, 4, 7]. Even though the spectrum of the microphone signals shows a lot more noise, presumably due to the minimal quantity lubrication (MQL), chatter frequencies could reliably be found. More frequency contents can be seen in the spectrum of the force signals. The most significant is the cutting edge engagement frequency. Others are the spindle frequency and its multiples. All decisions as to whether an operation point is stable or unstable could be made from measurements from both devices yielding the same result.

Considering the large number of measured data a way of clearly representing the chatter frequencies is needed. For this purpose, the Campbell diagram is predestinated. Here, the chatter frequencies at different spindle speeds are visualized. Spindle speed dependencies of the chatter frequencies and possible causes for non-linearities or other phenomena can be analyzed in detail. Figure 12.12 shows Campbell diagrams for unstable operating points between 26,000 rpm and 33,000 rpm.

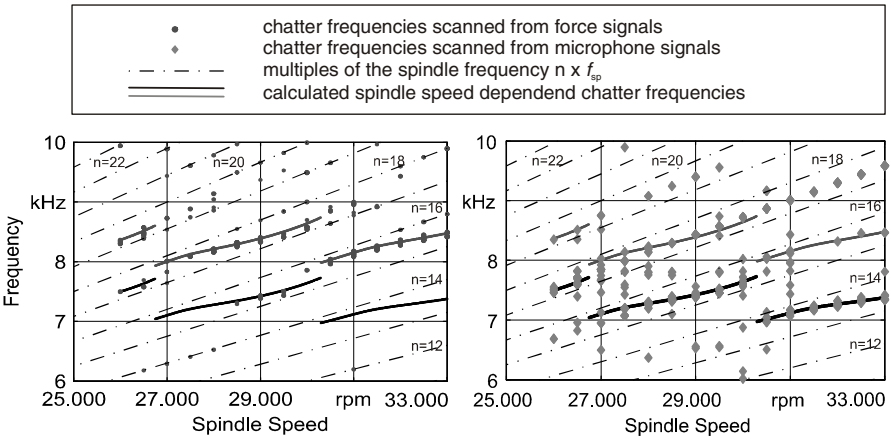

Fig. 12.12. Campbell diagrams from the force (left) and microphone spectra (right)

The parallel dashed lines signify the multiples of the spindle frequency. Especially in the Campbell diagram of the force signal it can be seen that some frequencies are located on those lines. All frequencies between the dashed lines are possible chatter frequencies. According to the theory of possible Hopf chatter frequencies [7], the chatter frequencies correspond to basic eigenfrequencies between 7 kHz and 7.2 kHz, which is presumably caused by the STT system. Therefore, the chatter frequencies are compared to calculated spindle-speed-dependent chatter frequencies. A good accordance can be stated for both diagrams. However, the microphone spectra are considered to be the superior method for chatter detection. Figure 12.13 shows the analytically computed stability charts, calculated by using the previously detected chatter frequencies, as well as the experimentally determined stability charts.

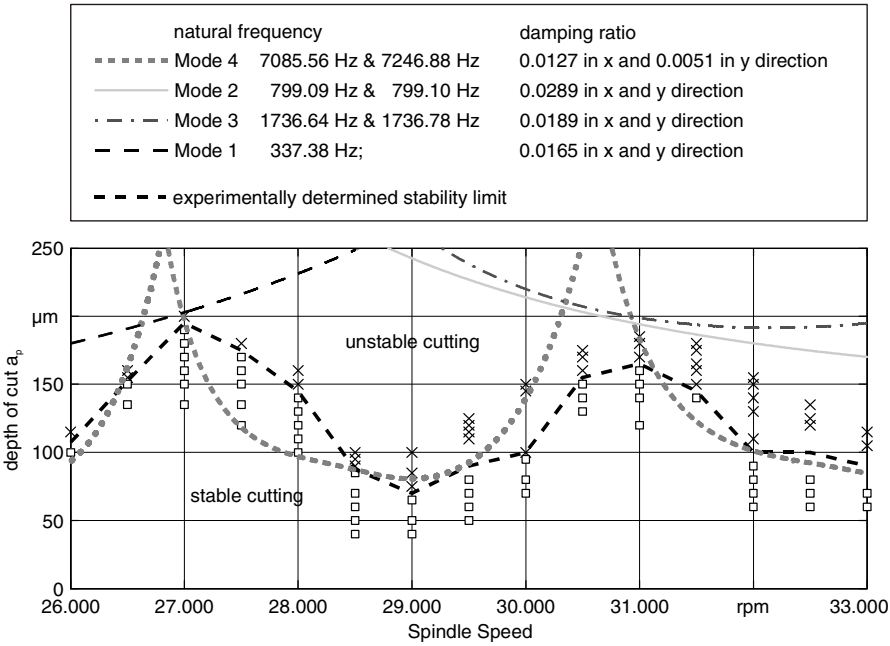

Fig. 12.13 Experimentally determined stability chart and simulated stability lobes with different chatter frequencies

It can be seen that the fourth mode of the machine tool model is dominant. The measured basic chatter frequency corresponds to this mode. The asymmetric modeling in x and y-directions also takes the mode interaction into account. Influences of other modes cannot directly be determined from the chatter frequencies due to their small significance compared to the fourth mode. However, their effects can be observed from the milled surfaces as shown in Figure 12.14.

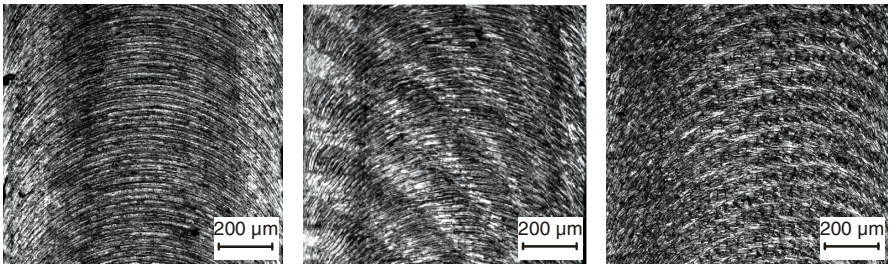

Fig. 12.14 Milled surfaces with stable cutting conditions at 28,000 rpm (left), unstable cutting conditions at 31,000 rpm (middle) and at 29,000 rpm (right)

The milled surface with stable conditions shows steady traces of the cutting edge trajectories. In contrast to that, unstable cutting conditions lead to different surfaces. Effects of overlaid vibrations can be seen additionally to the kinematic of the cutting edge trajectories. At 29,000 rpm, high-frequent deviations of the TCP

are reasons for that. This corresponds to the fourth mode above of 7 kHz. At 31,000 rpm, a waviness caused by lower frequent vibrations can be seen. It is supposed to be caused by the first three modes.

The chatter frequencies as seen in Figure 12.11 and Figure 12.12 vary in their magnitude as well as in their frequency value. One reason for that are changing conditions of the cutting process and the machine tool structure. Analyses of the tool holder and the clamping conditions are carried out in order to point out the most significant influences. Figure 12.15 shows the run-out as a function of the spindle speed measured at the tool shank. Also, the chatter frequencies at different clamping conditions are analyzed.

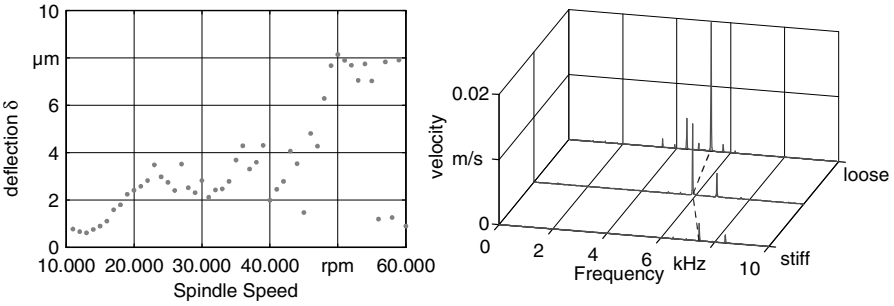

Fig. 12.15 Run-out as a function of spindle speed (left) and chatter frequency of the end mill at different clamping conditions (right)

It can be seen that the tool run-out is strongly influenced by the spindle speed. Therefore, the consideration of this effect within the comprehensive model is necessary. High magnitudes of frequencies, also at odd multiples of the spindle, and tool engagement frequency in force can be explained by that.

A significant influence on the dominant chatter frequency depending on the clamping conditions of the tool can also be stated. The difference of the chatter frequency can amount up to 2 kHz, which strongly affects the calculation of the stability chart.

12.4 Optimization

As depicted in the preceding section, chatter frequencies strongly depend on the variation of tool clamping and process conditions. This complicates the analytical determination of stability charts. A reliable method to identify chatter frequencies without extensively repeating the milling operations at different depths of cut a_p would therefore be helpful. For this purpose, an experimental set-up is illustrated in Figure 12.16.

Piezo-ceramic actuators are clamped between the workpiece and the clamping vice on the machine tool. The workpiece is excited with different signals during the milling process in order to evoke chatter.

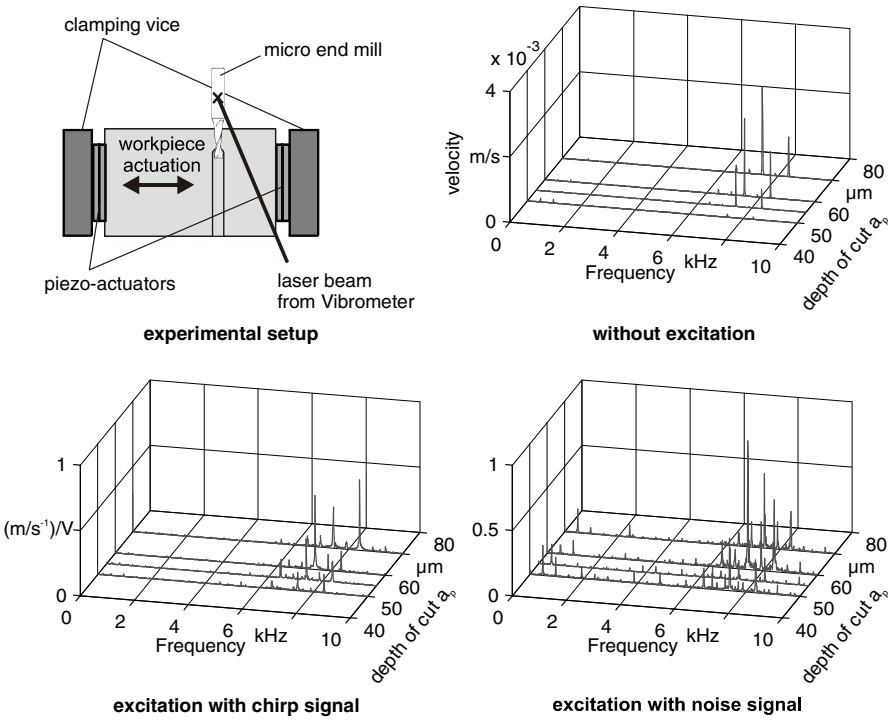

Fig. 12.16 Workpiece excitation by piezo-actuators

During the milling operation, the velocity of the micro end mill is measured using a laser vibrometer. Chatter frequencies can be determined from the spectra of the velocity of the end mill as soon as the process reaches the critical depth of cut a_p (in this case $a_p = 60$ µm). When a chirp signal is applied to the piezo-actuators the chatter frequencies can already be detected from the frequency response function (velocity/voltage) at a depth of cut of $a_p = 50$ µm. The similar phenomenon is also observed using noise signals as excitation, with more frequency contents, however.

Thus, this method allows the location of chatter frequencies at a very early stage of instability. Furthermore, no measurement equipment has to be applied, which possibly changes the dynamic behavior. The intended milling parameters can be used and the tool wear can be reduced compared to conventional methods.

12.5 Conclusion

This chapter has presented both analytical and experimental studies on the process stability of micro-milling . Experimental modal analyses of the machine tool structure as well as of the end mill were carried out. Subsequently, a comprehensive model including the machine tool dynamics as well as the process forces, was developed in order to calculate stability charts. The model includes rotational and

gyroscopic effects of the spindle-tool holder-tool-system (STT). The model for the dynamic process forces is based on a geometrical description of the cutting process. Influences of the helix angle as well as the cutting edge radius were taken into account. Experimental determinations of the specific cutting forces were then carried out to complete a preliminary parameter identification.

Using the model, calculated and experimentally determined stability charts were compared. Measured force, acoustic and optical signals were analyzed and employed as chatter criterion. The spindle speed dependence of the chatter frequencies were visualized in Campbell diagrams in order to verify the basic chatter frequencies. It is noticeable that the first bending resonance frequency of the analyzed end mills under stiff clamping conditions was detected at 8.7 kHz whereas the measured chatter frequencies during the milling process were between 7 kHz and 8.5 kHz. It can therefore be concluded that the chatter frequencies are not only due to the dynamic behavior of the end mill but arise from complex interactions of the structure eigenfrequencies. Measurements of the milled surfaces confirm this presumption. Since the chatter frequencies significantly influence the stability of the system, experiments on the tool run-out and the clamping conditions of the tool holder were carried out. Divergences of the chatter frequencies of up to 2 kHz were detected. As a result of the sensitive dynamic behavior an experimental setup for chatter detection was introduced. The workpiece was excited with different signals by piezo-electric actuators. Thereby, a reliable in-situ detection of the chatter frequencies without modifying the dynamic system (e. g. by the use of additional measurement equipment) could be realized.

References

[1] Altintas, Y., Budak, E.: Analytical prediction of stability lobes in milling. CIRP Annals 44, 357–362 (1995)

[2] Bayly, P.V., Halley, J.E., Mann, B.P., Davies, M.A.: Stability of interrupted cutting by temporal finite element analysis. ASME J. Manuf. Sci. Eng. 125, 220–225 (2003)

[3] Brammertz, P.H.: Die Entstehung der Oberflächenrauheit beim Feindrehen- Bericht aus dem Laboratorium für Werkzeugmaschinen und Betriebslehre der TH Aachen, Industrie-Anzeiger, Essen, Nr.2, pp. 25–32 (1961)

[4] Budak, E., Altintas, Y.: Analytical Prediction of Chatter Stability Conditions for Multidegree of Freedom Systems in Milling. Part I: General Formulation, Part II: Application of the General formulation to Common Milling Systems. Transactions of the ASME J. Eng. Ind. 120, 22–36 (1998)

[5] Duarte, M.L.M., Ewins, D.J.: Rotational degrees of freedom for structural coupling analysis via finite-difference technique with residual compensation. Mech. Syst. Signal Process 14(2), 205–227 (2000)

[6] Filiz, S., Ozdoganlar, O.B.: A three-dimensional model for the dynamics of microendmills including bending, torsional and axial vibrations. Precis. Eng. 35, 24–37 (2011)

[7] Insperger, T., Stépán, G.: Updated semi-discretization method for periodic delay-differential equations with discrete delay. Int. J. Numer. Methods Eng. 61, 117–141 (2004)

[8] Jun, M.B.G., DeVor, R.E., Kapoor, S.G.: Investigation of the Dynamics of Microend Milling—Part II: Model Validation and Interpretation. ASME J. Manuf. Sci. Eng. 128, 901–912 (2006)
[9] Kienzle, O., Victor, H.: Spezifische Schnittkräfte bei der Metallbearbeitung. Werkstatttechnik und Maschinenbau 47(5), 224–225 (1957)
[10] L'Vov, N.P.: Determining the minimum possible Chip-Thickness. Machines & Tooling 40(4), 45–46 (1968)
[11] Malekian, M., Park, S.S., Jun, M.B.G.: Investigation of Critical Chip Thickness and Micro Ploughing Forces. In: Proceedings of CIRP 2nd International Conference on Process Machine Interactions, Vancouver, Canada (2010)
[12] Mascardelli, B.A., Park, S.S., Freiheit, T.: Substructure coupling of microend mills to aid in the suppression of chatter. ASME J. Manuf. Sci. Eng. 130, 011010 (2008)
[13] Moriwaki, T., Shamoto, E.: Ultraprecision Ductile Cutting of Glass by Applying Ultrasonic Vibration. Annals of the CIRP 41(1), 141–144 (1992)
[14] Nelson, H.D., McVaugh, J.M.: The dynamics of rotor-bearing systems using finite elements. ASME J. Eng. Ind. 98(2), 593–600 (1976)
[15] Schauer, K.: Entwicklung von Hartmetallwerkzeugen für die Mikrozerspanung mit definierter Schneide, Dissertation, TU Berlin (2006)
[16] Schmitz, T.L., Donaldson, R.R.: Predicting high-speed machining dynamics by substructure analysis. CIRP Ann. - Manuf. Technol. 49(1), 303–308 (2000)
[17] Shi, Y., Mahr, F., von Wagner, U., Uhlmann, E.: A spatial multiple degree of freedom machine tool model for micro milling simulation. In: Proc. 2nd CIRP-PMI, MM06, Vancouver (2010)
[18] Uhlmann, E., Mahr, F., Shi, Y., von Wagner, U., Eßmann, J.: Interactions between mechanical vibrations and surface roughness during the micro milling process. In: Proceedings of CIRP 1st International Conference on Process Machine Interactions, Hannover, Germany, pp. 978–973 (2008)
[19] Wauer, J.: Kontinuumsschwingungen. Vieweg+Teubner Verlag, Wiesbaden (2008)
[20] Yuan, Z., Zhou, M., Dong, S.: Effect of diamond tool sharpness on minimum cutting thickness and cutting surface integrity in ultraprecission machining. Journal of Materials Processing Technology 62, S.327–S.330 (1996)
[21] Zorzi, E.S., Nelson, H.D.: Finite element simulation of rotor-bearing systems with internal damping. ASME J. Eng. Power 99(1), 71–76 (1977)